Biophysical *Journal*
Biophysical Letter

Optimal Affinity Enhancement by a Conserved Flexible Linker Controls p53 Mimicry in MdmX

Wade Borcherds,[1,2] Andreas Becker,[3] Lihong Chen,[4] Jiandong Chen,[4] Lucía B. Chemes,[5,*] and Gary W. Daughdrill[1,2,*]

[1]Department of Cell Biology, Microbiology, and Molecular Biology and [2]Center for Drug Discovery and Innovation, University of South Florida, Tampa, Florida; [3]Drug Discovery Department and [4]Molecular Oncology Department, Moffitt Cancer Center, Tampa, Florida; and [5]Protein Structure-Function and Engineering Laboratory, Fundación Instituto Leloir and IIBBA-CONICET, Buenos Aires, Argentina

ABSTRACT MdmX contains an intramolecular binding motif that mimics the binding of the p53 tumor suppressor. This intramolecular binding motif is connected to the p53 binding domain of MdmX by a conserved flexible linker that is 85 residues long. The sequence of this flexible linker has an identity of 51% based on multiple protein sequence alignments of 52 MdmX homologs. We used polymer statistics to estimate a global K_D value for p53 binding to MdmX in the presence of the flexible linker and the intramolecular binding motif by assuming the flexible linker behaves as a wormlike chain. The global K_D estimated from the wormlike chain modeling was nearly identical to the value measured using isothermal titration calorimetry. According to our calculations and measurements, the intramolecular binding motif reduces the apparent affinity of p53 for MdmX by a factor of 400. This study promotes a more quantitative understanding of the role that flexible linkers play in intramolecular binding and provides valuable information to further studies of cellular inhibition of the p53/MdmX interaction.

Mdm2 and MdmX (also known as Mdm4) are arguably the most important regulators of p53, being responsible for generating the dynamic characteristics of the p53 signaling pathway (1). Mdm2 is a classic p53 target gene and it was recently shown that p53 also induces MdmX transcription (2,3). Both Mdm2 and MdmX form negative feedback loops that regulate p53 activity using different mechanisms and mouse models show that Mdm2 and MdmX are necessary for controlling p53 activity (4–9). Mdm2 and MdmX contain N-terminal domains that bind tightly to residues 17–29 of the p53 transcriptional activation domain (p53TAD). MdmX also contains a short linear binding motif between residues 195–206 that resembles residues 17–29 of p53TAD. This motif interacts with the p53 binding domain (p53BD) of MdmX and interferes with p53 binding (10,11). We recently showed that a short peptide containing MdmX residues 195–206 binds to the p53BD of MdmX with a $K_D = 8.3 \pm 0.1\ \mu M$ (11). Based on this previous work, we hypothesize the intramolecular binding motif at residues 195–206, referred to as the WW motif because it contains two tryptophan residues, is connected to the p53-binding domain of MdmX by a long flexible linker that controls the intramolecular binding affinity. This hypothesis is supported by the IUPred disorder prediction of human MdmX shown in Fig. 1 *a* (12). IUPred correctly predicts the p53 binding domain of MdmX is ordered (13,14). After the p53 binding domain is a long segment from residues 112–181 predicted to be disordered, and a short segment from residues 182–211, which includes the WW motif, with disorder tendency values that dip below 0.5. Previous studies have shown that short protein segments with a disorder tendency <0.5 will often correspond to linear binding motifs (15–17). In the case of MdmX, the binding of this linear motif is intramolecular. It is also worth noting that ANCHOR correctly predicts the WW motif is a protein binding site (18).

The disorder prediction shown in Fig. 1 *a* provides a useful global assessment of disorder propensity but it lacks the resolution to determine the physical boundaries of the MdmX linker at the single amino acid level. To determine the C-terminal boundary of the linker, we analyzed a recent study published by Fersht and colleagues, where NMR spectroscopy was used to characterize the interaction between the p53BD of MdmX (residues 1–111) and a ^{15}N-labeled peptide containing the WW motif (residues 181–209) (10). In the ^{15}N-HSQC spectrum of this peptide bound to the p53BD of MdmX, resonances for residues 195–204 disappear but the resonance for residue 194 is still detectable. It is not as strong as the resonance in the free peptide, but it is clearly visible and does not shift its position. Based

Submitted January 19, 2017, and accepted for publication April 17, 2017.
*Correspondence: gdaughdrill@usf.edu or lchemes@leloir.org.ar
Editor: Rohit Pappu.
http://dx.doi.org/10.1016/j.bpj.2017.04.017

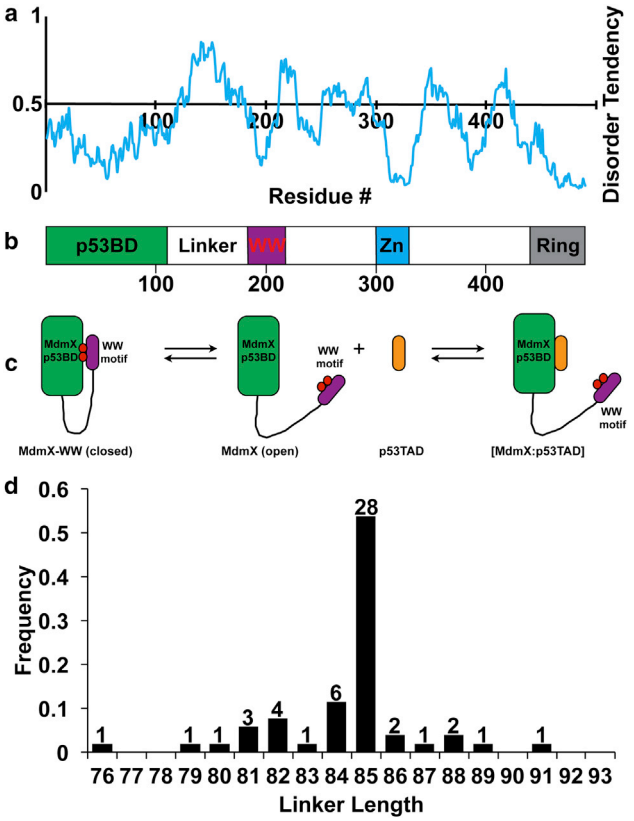

FIGURE 1 MdmX has a conserved flexible linker. (*a*) Plot showing IUPred disorder prediction of human MdmX. (*b*) Domain schematic of human MdmX showing position of p53 binding domain (p53BD), the linker, and the WW motif. The residue numbers in the disorder prediction are aligned with the domain schematic. (*c*) Model showing competition between the WW motif and p53TAD for the p53BD. (*d*) Histogram showing the distribution of lengths for the flexible linkers of 52 MdmX homologs based on a multiple protein sequence alignment that included 10 primates, 24 other mammals, 4 birds, 1 amphibian, 1 reptile, and 12 fish. The number of species in each bin is shown above the bars.

on these observations, we conclude the C-terminal boundary of the linker is at residue 194. To determine the N-terminal boundary of the linker, we examined the structure of human MdmX (residues 23–111) bound to a p53 peptide (residues 15–29; PDB: 3DAB) (14). Residue 109 of MdmX is the last amino acid observed in this structure. This means that residues 110 and 111 are flexible and do not produce coherent scattering in the x-ray diffraction pattern. Based on this observation, starting the linker at residue 110 seems reasonable. Including residues 110 and 194 makes the linker 85 residues long. It is no great surprise that the last two residues in a crystal structure are not resolved, but as we show below, changing this length by ±4 residues has a minimal effect on the predicted strength of intramolecular binding.

Using the linker boundaries described above, we performed multiple protein sequence alignments on 52 MdmX homologs (Fig. S1). Based on the sequence identity matrix calculated from the alignments, the overall sequence identity is 51%. A histogram showing the length distribution of the linkers from the 52 homologs is presented in Fig. 1 *d*. A total of 48 of the 52 (92%) homologs have a length of 85 ± 4 residues. The shortest linker length is 76 residues (frog) and the longest is 91 residues (opossum). Based on this analysis, we conclude both the length and sequence of the linker is highly conserved in vertebrates.

Flexible linkers represent a functionally important class of intrinsically disordered regions. They can modulate the distance between multiple inter- or intramolecular protein-binding sites and this, in turn, can modulate binding affinity. In some cases, this behavior can be predicted by the wormlike chain (WLC) model initially proposed by Zhou and co-workers (19–24). The WLC model describes semiflexible polymers like IDPs using two variables—a contour length (L_c) and a persistence length (L_p). For a fixed chain length, higher values of L_c and L_p lead to more extended conformations (20,22). L_c is the length of a fully extended chain with a certain number of monomers. L_p is a measure of polymer stiffness and corresponds to the distance necessary for the direction of the chain to become uncorrelated. For our modeling, $L_c = N_{res} \times 3.8$ Å, where N_{res} is the number of residues in the linker, and 3.8 Å is the distance per residue and $L_p = 3$ Å. These values provide a good approximation for the behavior of polypeptides (20). We used the WLC model to estimate the probability of end-to-end distances for the MdmX linker region and the effective concentration (C_{eff}) for the WW motif at the p53BD of MdmX (Supporting Material, Eqs. S1–S3). C_{eff} represents the concentration of one linker end at a fixed distance from the site of tethering. For a fixed distance, C_{eff} gradually increases with linker length up to a maximal value, and then decreases slowly for longer linkers (20,22).

The probability distribution of end-to-end distances, $p(r)$, for an 85-residue linker had a maximum at 36 Å (Fig. 2). If we assume a binding orientation for the WW motif that is similar to the p53TAD peptide shown in Fig. 2 *a*, 36 Å is very close to the observed separation of 38 Å between the end of the p53BD (residue 109) and the putative beginning of the WW motif (14). Because 92% of the homologs used to make the histogram in Fig. 1 *d* have linker lengths from 81 to 89 residues, we calculated $p(r)$ for 81- and 89-residue linkers. The values are 35.5 and 37 Å, respectively, which are also very close to the experimentally measured distance of 38 Å.

To estimate the effective concentration (C_{eff}) of the WW motif at the p53BD of MdmX, we used the most probable linker length of 85 residues and a separation distance between the end of the p53 binding domain and the beginning of the WW motif of 38 Å (Supporting Material; Eq. S3). Using these values, we calculated a C_{eff} value of 2.12 mM. This C_{eff} value, along with the previously

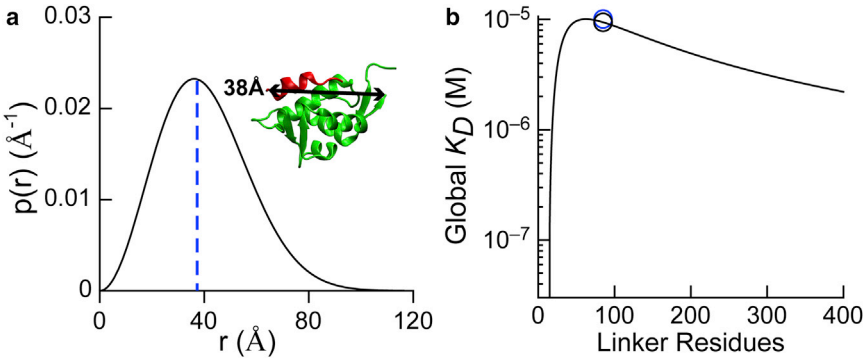

FIGURE 2 Modeling MdmX intramolecular interactions using polymer statistics. (*a*) Shown here is the probability distribution of end-to-end distances for the MdmX linker region (residues 110–194). The distribution peaks at 36 Å are given. The blue dashed line marks 38 Å, the measured distance between the end of the MdmX domain and the beginning of the WW motif considering the same binding orientation as p53TAD, measured from PDB: 3DAB. The ribbon model shows a structure from PDB: 3DAB. (*b*) Shown here is the predicted global K_D as a function of linker length for a direct binding orientation model. Black circle: global K_D predicted by the WLC model for an 85-residue linker; blue circle: experimentally measured global K_D (see Fig. 3).

determined bimolecular association constant for a short peptide corresponding to the WW motif binding to the p53BD of MdmX (11), was used to calculate the intramolecular association constant, K_A', and the fraction of the MdmX molecules that are in the closed conformation shown in Fig. 1 *c* (Supporting Material; Eqs. S4 and S5). According to these equilibrium calculations, the fraction of MdmX molecules in the closed conformation is 0.996, which corresponds to a K_A' value of 255. Using K_A', we calculated the global dissociation constant for the binding of p53TAD to a fragment of MdmX containing the p53BD, the linker, and the WW motif (residues 23–210) (Supporting Material; Eqs. S6 and S7). For this calculation, we considered the two equilibrium reactions illustrated in Fig. 1 *c*. The first equilibrium reaction is between the closed and open conformations where the WW motif is respectively bound and not bound to the p53BD. In the second equilibrium reaction, $MdmX_{23–210}$ is in the open conformation and p53TAD is bound to the p53BD. The predicted global K_D reached a maximum value for a linker length of 62 residues (Fig. 2 *b*). This is the length at which p53 binding is maximally compromised by the autoinhibitory effects of the WW motif binding to the p53BD. Using a linker length of 85 residues, we calculate a global $K_D = 9.4 \pm 1.5$ μM for p53TAD binding to $MdmX_{23–210}$. The global K_D values we estimated for 81 and 89 residue linkers are 9.6 and 9.3 μM, respectively. Our modeling suggests that the intramolecular binding affinity achieved by an 85 residue linker is close to the maximum and that the range of linker lengths observed for the homologs will all have a similar autoinhibitory effect on p53 binding.

Fig. 3 shows the results from isothermal titration calorimetry (ITC) experiments for two fragments of MdmX binding to a fragment of the p53 transactivation domain that contains residues 1–73 (p53TAD). Fig. 3 *a* shows the fitted ITC data for p53TAD binding to $MdmX_{23–111}$. We observe a $K_D = 25 \pm 3$ nM. p53TAD binds more tightly to $MdmX_{23–111}$ than the short peptide corresponding to p53 residues 17–28 used for previous structural studies (25–27). This tighter binding is due to additional interactions between $MdmX_{23–111}$ and p53 residues 29–32 (10). Fig. 3 *b* shows the K_D for p53TAD binding to $MdmX_{23–210}$ dramatically increases to a value of 10 ± 1 μM due to the addition of the WW motif. Fig. S2 shows ITC data for longer MdmX fragments that lack the WW motif. As expected, the WW motif interferes with the binding of p53TAD to MdmX, reducing the apparent binding affinity by 400-fold. The experimentally obtained K_D value is in very close agreement with the K_D of 9.4 ± 1.5 μM predicted by the C_{eff} values obtained using the WLC model. The agreement between the experimentally measured K_D and the value predicted using the WLC model suggests that the MdmX linker behaves as a flexible polymer that enhances the intramolecular binding of the WW motif. This intramolecular binding competes with the binding of p53, reducing its apparent affinity for MdmX by two orders of magnitude. The fact the 92% of

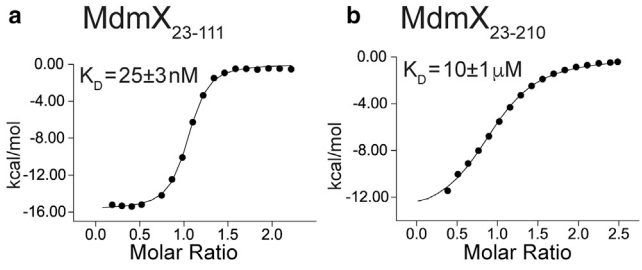

FIGURE 3 Plots showing p53TAD binding to fragments of MdmX with and without the flexible linker and WW motif. Black circles show enthalpy per mole of injectant, measured using isothermal titration calorimetry, plotted as a function [p53TAD]/[MdmX]. Black lines show the fit to the data using a single site binding model. (*a*) Shown here is p53TAD binding to $MdmX_{23–111}$. (*b*) Shown here is p53TAD binding to $MdmX_{23–210}$.

the homologs we analyzed have a linker length that is within four amino acids of the human homolog suggests the linker length and the intramolecular affinity enhancement are conserved. These results have important implications for our understanding of p53 regulation and help to explain previous results from the Chen group showing that CK1α copurifies with MdmX by binding to the acidic domain and stimulating MdmX-p53 binding (28). It is not clear exactly where CK1α binds to MdmX, but we hypothesize it is positioned to interfere with intramolecular binding of the WW motif, allowing p53TAD to access the p53BD of MdmX (11). Our work also suggests that the MdmX linker has evolved to promote optimal positioning of the WW motif for binding to the p53BD. Finally, we think our work adds support for the use of WLC modeling of disordered regions that act mainly as flexible tethers (21–24). To improve the accuracy of this modeling, additional variables, such as sequence patterning (see CIDER analysis in Fig. S3) and tethering interactions, must ultimately be considered (29,30).

SUPPORTING MATERIAL

Supporting Materials and Methods and three figures are available at http://www.biophysj.org/biophysj/supplemental/S0006-3495(17)30433-2.

AUTHOR CONTRIBUTIONS

W.B. performed experiments, analyzed data, and wrote the manuscript. L.C. generated expression plasmids. J.C. designed experiments and edited the manuscript. L.B.C. performed polymer statistics calculations and edited the manuscript. G.W.D. managed the project, designed experiments, wrote the manuscript, and edited the manuscript.

ACKNOWLEDGMENTS

This work is supported in part by National Institutes of Health (NIH) grants Nos. GM115556 and CA141244 to G.W.D., NIH grants Nos. CA109636, CA141244, and CA186917 and Florida Department of Health grant No. 4BB14 to J.C., and Agencia Nacional de Promoción Científica y Tecnológica (ANPCyT) grant No. PICT-2013-1895 to L.B.C. The H. Lee Moffitt Cancer Center & Research Institute is a National Cancer Institute-designated Comprehensive Cancer Center through grant No. P30-CA076292.

REFERENCES

1. Wade, M., Y. C. Li, and G. M. Wahl. 2013. MDM2, MDMX and p53 in oncogenesis and cancer therapy. *Nat. Rev. Cancer.* 13:83–96.
2. Li, B., Q. Cheng, …, J. Chen. 2010. p53 inactivation by MDM2 and MDMX negative feedback loops in testicular germ cell tumors. *Cell Cycle.* 9:1411–1420.
3. Phillips, A., A. Teunisse, …, A. G. Jochemsen. 2010. HDMX-L is expressed from a functional p53-responsive promoter in the first intron of the HDMX gene and participates in an autoregulatory feedback loop to control p53 activity. *J. Biol. Chem.* 285:29111–29127.
4. Finch, R. A., D. B. Donoviel, …, N. Zhang. 2002. Mdmx is a negative regulator of p53 activity in vivo. *Cancer Res.* 62:3221–3225.
5. Grier, J. D., S. Xiong, …, G. Lozano. 2006. Tissue-specific differences of p53 inhibition by Mdm2 and Mdm4. *Mol. Cell. Biol.* 26:192–198.
6. Jones, S. N., A. E. Roe, …, A. Bradley. 1995. Rescue of embryonic lethality in Mdm2-deficient mice by absence of p53. *Nature.* 378:206–208.
7. Migliorini, D., E. Lazzerini Denchi, …, J. C. Marine. 2002. Mdm4 (Mdmx) regulates p53-induced growth arrest and neuronal cell death during early embryonic mouse development. *Mol. Cell. Biol.* 22:5527–5538.
8. Montes de Oca Luna, R., D. S. Wagner, and G. Lozano. 1995. Rescue of early embryonic lethality in mdm2-deficient mice by deletion of p53. *Nature.* 378:203–206.
9. Parant, J. M., V. Reinke, …, G. Lozano. 2001. Organization, expression, and localization of the murine mdmx gene and pseudogene. *Gene.* 270:277–283.
10. Bista, M., M. Petrovich, and A. R. Fersht. 2013. MDMX contains an autoinhibitory sequence element. *Proc. Natl. Acad. Sci. USA.* 110:17814–17819.
11. Chen, L., W. Borcherds, …, J. Chen. 2015. Autoinhibition of MDMX by intramolecular p53 mimicry. *Proc. Natl. Acad. Sci. USA.* 112:4624–4629.
12. Dosztányi, Z., V. Csizmók, …, I. Simon. 2005. The pairwise energy content estimated from amino acid composition discriminates between folded and intrinsically unstructured proteins. *J. Mol. Biol.* 347:827–839.
13. Sanchez, M. C., J. G. Renshaw, …, M. Vogtherr. 2010. MDM4 binds ligands via a mechanism in which disordered regions become structured. *FEBS Lett.* 584:3035–3041.
14. Popowicz, G. M., A. Czarna, and T. A. Holak. 2008. Structure of the human Mdmx protein bound to the p53 tumor suppressor transactivation domain. *Cell Cycle.* 7:2441–2443.
15. Oldfield, C. J., Y. Cheng, …, A. K. Dunker. 2005. Coupled folding and binding with α-helix-forming molecular recognition elements. *Biochemistry.* 44:12454–12470.
16. Davey, N. E., K. Van Roey, …, T. J. Gibson. 2012. Attributes of short linear motifs. *Mol. Biosyst.* 8:268–281.
17. Mészáros, B., Z. Dosztányi, and I. Simon. 2012. Disordered binding regions and linear motifs—bridging the gap between two models of molecular recognition. *PLoS One.* 7:e46829.
18. Mészáros, B., I. Simon, and Z. Dosztányi. 2009. Prediction of protein binding regions in disordered proteins. *PLoS Comput. Biol.* 5:e1000376.
19. Zhou, H. X. 2001. Loops in proteins can be modeled as worm-like chains. *J. Phys. Chem. B.* 105:6763–6766.
20. Zhou, H. X. 2004. Polymer models of protein stability, folding, and interactions. *Biochemistry.* 43:2141–2154.
21. Zhou, H. X. 2006. Quantitative relation between intermolecular and intramolecular binding of pro-rich peptides to SH3 domains. *Biophys. J.* 91:3170–3181.
22. Bertagna, A., D. Toptygin, …, D. Barrick. 2008. The effects of conformational heterogeneity on the binding of the Notch intracellular domain to effector proteins: a case of biologically tuned disorder. *Biochem. Soc. Trans.* 36:157–166.
23. Krishnamurthy, V. M., V. Semetey, …, G. M. Whitesides. 2007. Dependence of effective molarity on linker length for an intramolecular protein-ligand system. *J. Am. Chem. Soc.* 129:1312–1320.
24. van Valen, D., M. Haataja, and R. Phillips. 2009. Biochemistry on a leash: the roles of tether length and geometry in signal integration proteins. *Biophys. J.* 96:1275–1292.
25. Pazgier, M., M. Liu, …, W. Lu. 2009. Structural basis for high-affinity peptide inhibition of p53 interactions with MDM2 and MDMX. *Proc. Natl. Acad. Sci. USA.* 106:4665–4670.

26. Phan, J., Z. Li, …, J. Chen. 2010. Structure-based design of high affinity peptides inhibiting the interaction of p53 with MDM2 and MDMX. *J. Biol. Chem.* 285:2174–2183.

27. Popowicz, G. M., A. Dömling, and T. A. Holak. 2011. The structure-based design of Mdm2/Mdmx-p53 inhibitors gets serious. *Angew. Chem. Int. Ed. Engl.* 50:2680–2688.

28. Chen, L., C. Li, …, J. Chen. 2005. Regulation of p53-MDMX interaction by casein kinase 1α. *Mol. Cell. Biol.* 25:6509–6520.

29. Das, R. K., and R. V. Pappu. 2013. Conformations of intrinsically disordered proteins are influenced by linear sequence distributions of oppositely charged residues. *Proc. Natl. Acad. Sci. USA.* 110: 13392–13397.

30. Sherry, K. P., S. E. Johnson, …, D. Barrick. 2015. Effects of linker length and transient secondary structure elements in the intrinsically disordered Notch RAM region on Notch signaling. *J. Mol. Biol.* 427:3587–3597.

Biophysical Journal, Volume *112*

Supplemental Information

Optimal Affinity Enhancement by a Conserved Flexible Linker Controls p53 Mimicry in MdmX

Wade Borcherds, Andreas Becker, Lihong Chen, Jiandong Chen, Lucía B. Chemes, and Gary W. Daughdrill

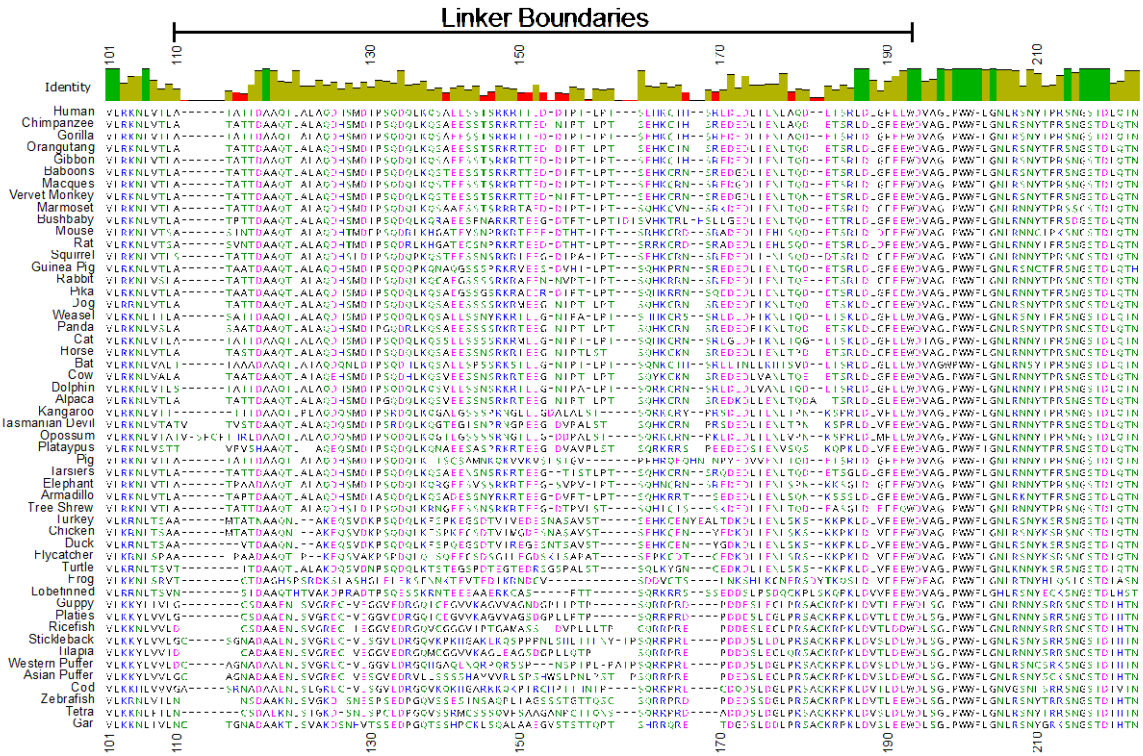

Figure S1: **Multiple protein sequence alignment of the MdmX linker from 52 MdmX homologues** including 10 primates, 24 other mammals, 4 birds, 1 amphibian, 1 reptile, and 12 fish. This alignment was used to generate the histogram in Figure 1.

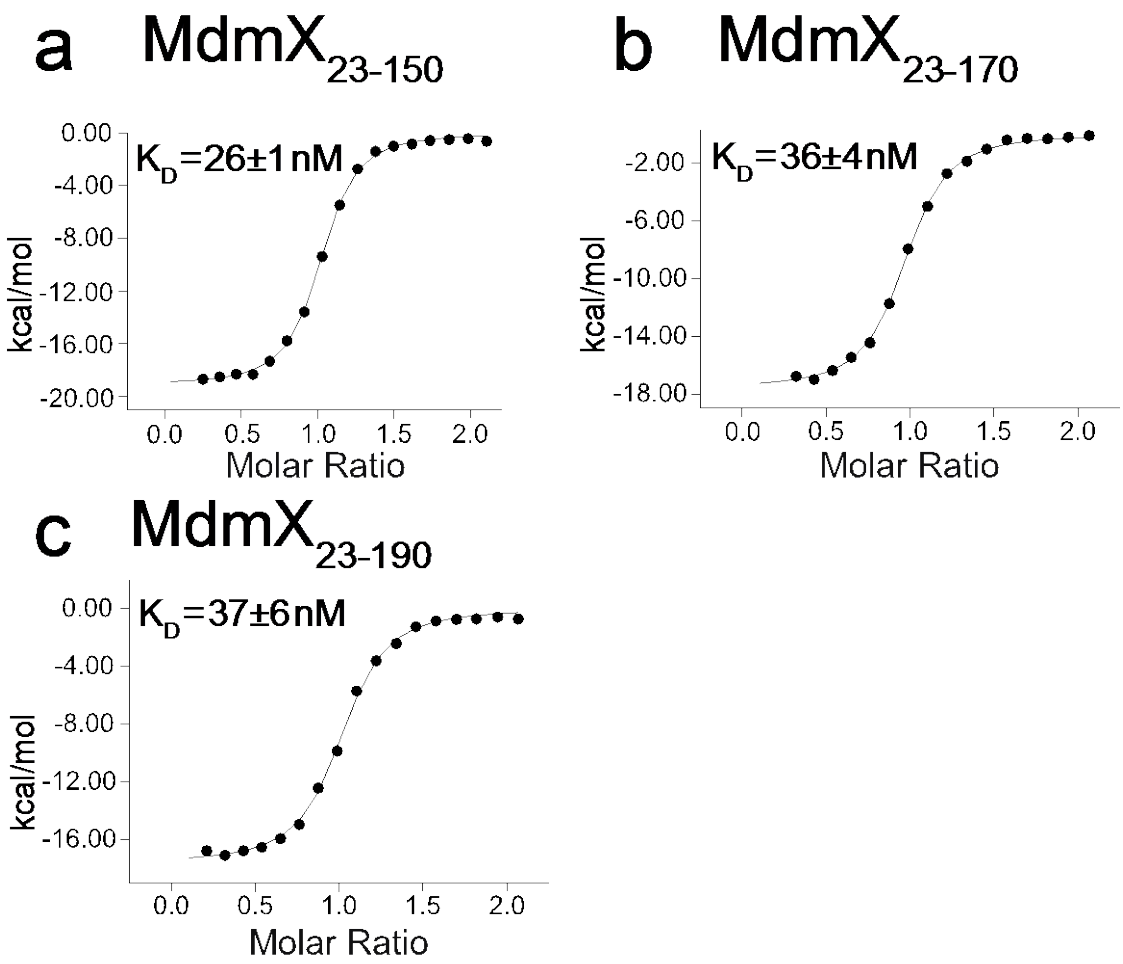

Figure S2: **p53TAD binding to fragments of MdmX with different lengths of the flexible linker.** Black circles show enthalpy per mole of injectant, measured using isothermal titration calorimetry, plotted as a function [p53TAD]/[MdmX]. Black lines show the fit to the data using a single site binding model. a. p53TAD binding to $MdmX_{23-150}$. b. p53TAD binding to $MdmX_{23-170}$. c. p53TAD binding to $MdmX_{23-190}$.

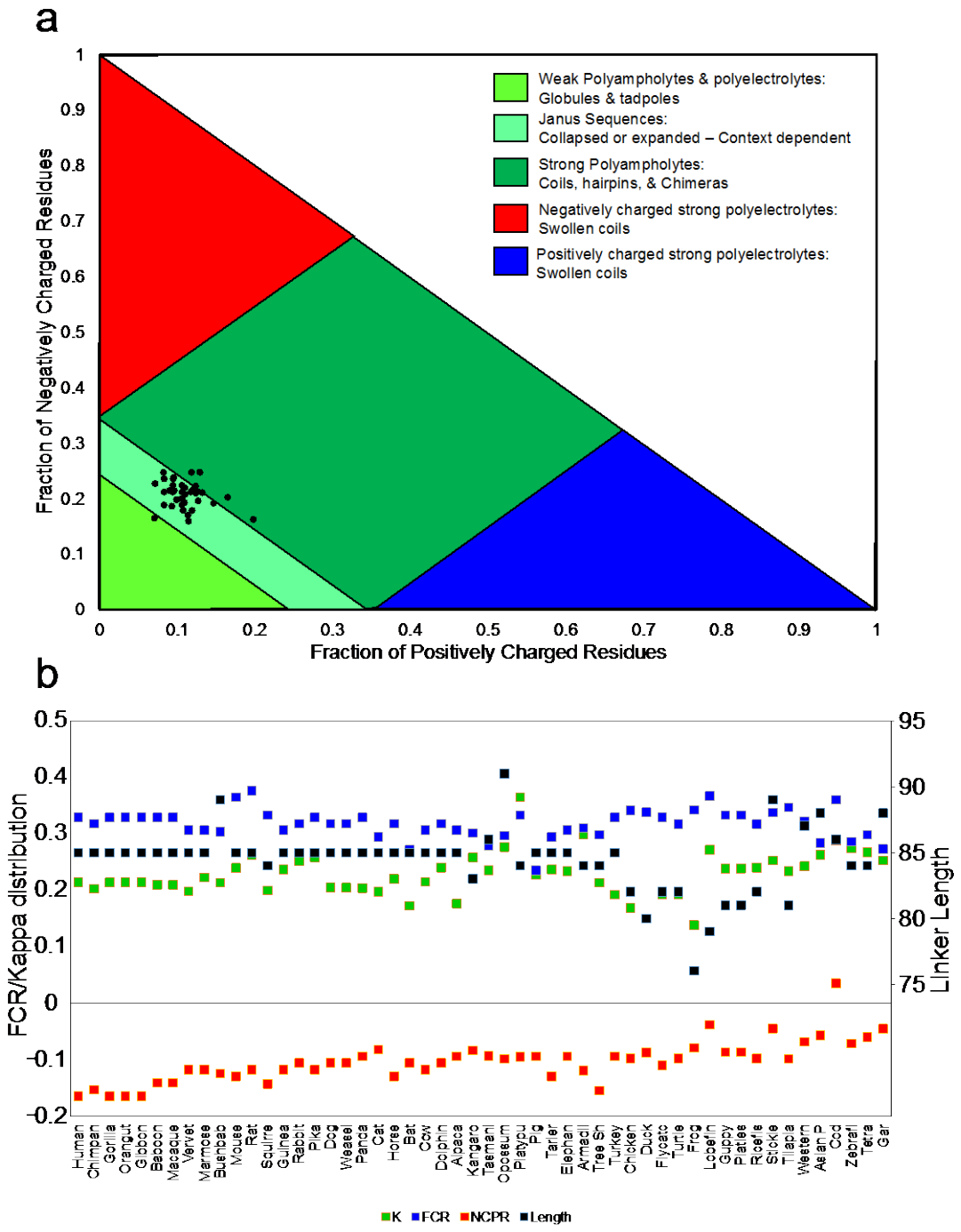

Figure S3: **CIDER analysis for MDMX linker sequences.** a. Diagram of states, the orthologues are primarily clustered within the Janus sequence zone of the plot. b. plot showing Kappa charge distribution value (K) in green, fraction of charged residues (FCR) in blue, net charge per residue (NCPR) in red, and the linker length in black for each of the MdmX orthologues. See reference 1.

Wormlike chain (WLC) modeling of the MdmX linker region

To model the behavior of the MdmX linker we used a previously described wormlike chain model that considers a polypeptide chain to behave as a continuous cylinder with a fixed but randomly directed radius of curvature (2,3). In this model, the end-to-end distribution depends only on two parameters, the persistence length *Lp* (length it takes for the motions to become uncorrelated) and the contour length *Lc* (total length of the chain). For our calculations, we used a persistence length *Lp* = 3Å which has been used previously for aminoacid chains [Zhou, 2004] and *Lc* = N_{res}*3.8 Å, where N_{res} is the number of residues in the linker (in this case 85), and 3.8 Å is the distance per chain element, in this case one amino acid.

P(r) calculations: The distribution function for the end-to-end distances can be written as

$$p(r) = 4\pi r^2 \left(\frac{3}{4\pi L_p L_c}\right)^{\frac{3}{2}} exp\left(\frac{-3r^2}{4L_p L_c}\right) \zeta\left(r, L_p, L_c\right) \quad [1]$$

Where the last term is defined as:

$$\zeta\left(r, L_p, L_c\right) = 1 - \left\{\frac{5L_p}{4L_c} - \frac{2r^2}{{L_c}^2} + \frac{33r^4}{80L_p{L_c}^3} + \frac{79{L_p}^2}{160{L_c}^2} + \frac{329L_p r^2}{120{L_c}^3} - \frac{6799r^4}{1600{L_c}^4} + \frac{3441r^6}{2800L_p{L_c}^5} - \frac{1089r^8}{12800{L_p}^2{L_c}^6}\right\} \quad [2]$$

C_{eff} calculations: The effective concentration in the bound state when the linker is restrained to a distance between binding sites r_o can be expressed as:

$$C_{eff} = \frac{p(r_o)}{4\pi r^2} \frac{10^{27} Å^3 l^{-1}}{L_o} \quad [3]$$

Where L_o is Avogadro's number, and C_{eff} is expressed in molar units. Multiplying Eq. [3] by 10^3 gives C_{eff} in millimolar units.

<u>Equilibrium scheme used for WLC modeling of binding affinity enhancement for the MdmX linker.</u>

We used the following equilibria to model the MdmX intramolecular interaction, and the MdmX-p53 interactions

I- Model for bimolecular interaction of WW with MdmX

We define the first equilibrium as:

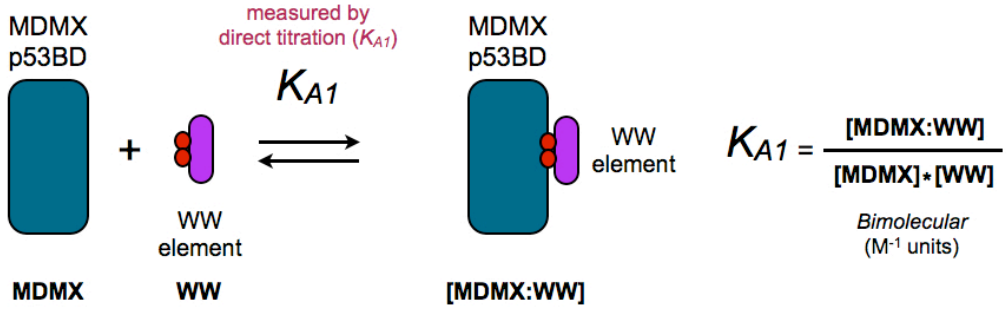

Where K_{A1} is the measured bimolecular association constant of the MdmX WW element to the MdmX p53 binding domain, in units of M^{-1}.

II- Model for intramolecular binding of WW to MdmX

We define the intramolecular MdmX equilibrium as:

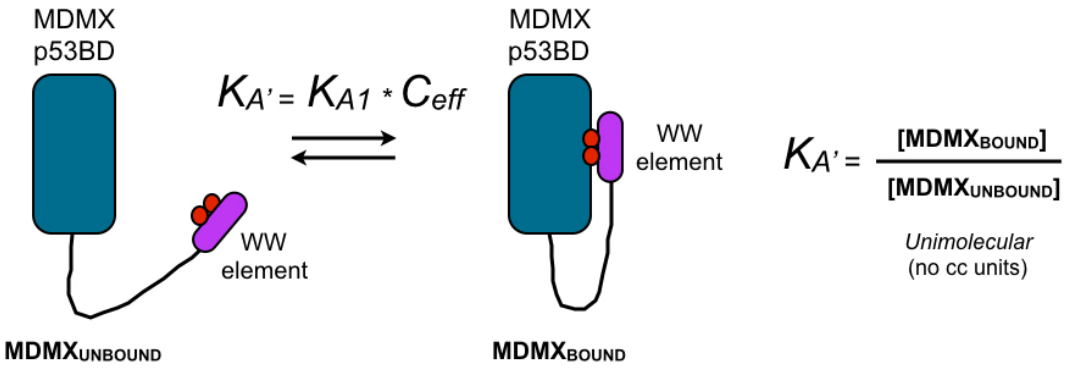

And

$$K_{A'} = K_{A1} * Ceff \qquad [4]$$

Where $K_{A'}$ is the intra-molecular binding constant, and C_{eff} is the effective concentration, which was estimated from the WLC model (Eqn. [1]-[3]). $K_{A'}$ is unimolecular and therefore has no concentration units.

III- Calculating populations of $MdmX_{UNBOUND}$ and $MdmX_{BOUND}$ from $K_{A'}$

From the definition of $K_{A'}$ = [$MdmX_{BOUND}$]/[$MdmX_{UNBOUND}$] we can calculate the fractional population of the $MdmX_{BOUND}$ and $MdmX_{UNBOUND}$ conformers as:

$$f_{MdmXBOUND} = \frac{K_{A'}}{1+K_{A'}}; f_{MdmXUNBOUND} = \frac{1}{1+K_{A'}} \qquad [5]$$

Which does not depend on the concentration of MdmX.

IV- ***Modeling the competition between P53TAD and WW for binding to MdMX***

Taking into account the previous equilibria, the binding of p53TAD to the MdmX variant containing the intramolecular motif can be modeled as follows:

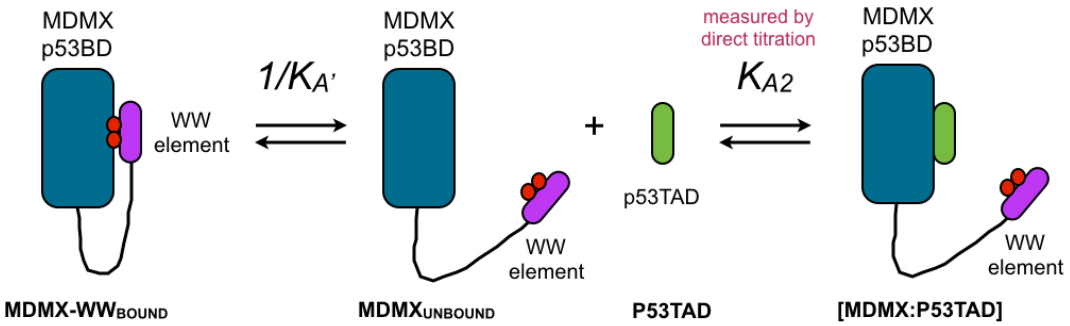

Where, based on measurements of the bimolecular association constant for binding of P53TAD to the MdmX domain without the intramolecular motif (K_{A2}), we can calculate the global equilibrium association constant for binding of p53TAD to the motif-containing MdmX construct as:

$$K_{A\ global} = \frac{1}{K_{A'}} * K_{A2} \qquad [6]$$

$$K_{D\ global} = K_{A'} * K_{D2} \qquad [7]$$

Note that K_D global = $K_{A'}$*K_{D2} and $K_{A'}$ = K_A*C_{eff}. This implies that higher values of C_{eff} lead to an increase in the global K_D value. This is equivalent to a decrease in the global binding affinity of p53TAD to MdmX. Therefore, higher values for C_{eff} lead to stronger MdmX intramolecular interactions and weaken P53TAD association to MdmX.

Supporting Material

Methods

Sequence Alignments

Mdmx alignments were carried out with the Geneious software suite version 10.0.7(4) using the ClustalW alignment algorithm (5) set to use the Blosum62 matrix with a gap open penalty of 12, extension penalty of 3, and 2 refinement iterations. The indicated residue numbers align with human mdmx.

Protein Expression and Purification

Mdmx cDNA constructs encoding residues 23-111, 23-150, 23-170, 23-190, and 23-210 were expressed using the pGEX-6p-2 vector transformed into BL21(DE3) cells and grown in minimal media. Overnight cultures were used to start cultures at OD600=0.04 and were grown to an OD600 of 0.6 and then induced with 1mM IPTG at 15 degrees Celsius for 16 hours. Pellets were re-suspended and lysed via French press in 50mM Tris, 300mM NaCl, 2.5mM EDTA, 1mM DTT, and 0.02% sodium azide pH 7.4 in the presence of ThermoScientific Pierce protease inhibitors (88665). GST tagged protein was then purified by passing the soluble fraction of lysate through a glutathione sepharose column (GE 17513201) and eluting with 10mM reduced glutathione. The GST tag was cleaved by incubation with the GST tagged HRV3C protease overnight at 4 Celsius, the glutathione was dialyzed away, and the cleaved tag was removed via a second glutathione sepharose column. The flowthrough is further purified via a superdex 75 SEC column (GE 28989333). The p53TAD construct encoding residues 1-73 in pET28A was prepared and purified as previously described (6).

Isothermal Titration Calorimetry

Mdmx and p53 polypeptides were co-dialyzed into 50mM NaPO4, 150mM NaCl, 1mM EDTA, 0.02% Sodium Azide, 8mM BME at pH 6.8. For mdmx constructs shorter than 23-210 3 replicate titrations were conducted with 2uM Mdmx in the cell and 20uM of p53 1-73 in the syringe using 15uL injections using a MicroCal-VP-ITC system at 25 celsius. For the 23-210 Mdmx construct 2 titrations were conducted using a MicroCal-ITC 200 system with 80uM Mdmx in the cell and 975uM of p53TAD 1-73 in the syringe using 2.05uL injections at 25 celsius. The corrected heat values were fit using Microcal origin software's (7.0) built in non-linear least square curve-fitting algorithm yielding the stoichiometry, enthalpy, and affinity constants reported.

1. Holehouse, A.S., Das, R.K., Ahad, J.N., Richardson, M.O.G., and Pappu, R.V. 2017. CIDER: Resources to Analyze Sequence-Ensemble Relationships of Intrinsically Disordered Proteins. Biophys. J. 112, 16-21.
2. Zhou, H. X. 2004. Polymer models of protein stability, folding, and interactions. Biochemistry 43:2141-2154.
3. Bertagna, A., D. Toptygin, L. Brand, and D. Barrick. 2008. The effects of conformational heterogeneity on the binding of the Notch intracellular domain to effector proteins: a case of biologically tuned disorder. Biochem. Soc. Trans. 36:157-166.
4. Kearse, M., Moir, R., Wilson, A., Stones-Havas, S., Cheung, M., Sturrock, S., Buxton, S., Cooper, A., Markowitz, S., Duran, C., Thierer, T., Ashton, B., Mentjies, P., & Drummond, A. 2012. Geneious Basic: an integrated and extendable desktop software platform for the organization and analysis of sequence data. *Bioinformatics*, *28*(12), 1647-1649.
5. Thompson, J. D., Higgins, D. G., & Gibson, T. J. 1994. CLUSTAL W: improving the sensitivity of progressive multiple sequence alignment through sequence weighting, position-specific gap penalties and weight matrix choice. *Nucleic Acids Research*, *22*(22), 4673–4680.
6. Vise, Pamela D. et al. "NMR Chemical Shift and Relaxation Measurements Provide Evidence for the Coupled Folding and Binding of the p53 Transactivation Domain." *Nucleic Acids Research* 33.7 (2005): 2061–2077.*PMC*. Web. 17 Oct. 2016.